CrystEngComm

Accepted Manuscript

ROYAL SOCIETY OF CHEMISTRY

www.rsc.org/crystengcomm

Dealloying induced plasmonic Au nanoparticles modified mesoporous TiO_2 for enhanced visible light photocatalysis

Zhengfeng Zhao, Xiaoxia Zhu, Min Zuo, Jing Xu and Yan Wang*

School of Materials Science & Engineering, University of Jinan, No. 336, West Road of Nan Xinzhuang, Jinan 250022, PR China

* Corresponding author. Tel: +86-531-82765473; Fax: +86-531-87974453

E-mail address: mse_wangy@ujn.edu.cn (Yan Wang).

Abstract

Plasmonic noble metallic nanoparticles have emerged as a promising material in sensitizing wide-bandgap semiconductors for visible-light photocatalysis. However, the preparation of plasmonic metallic nanoparticles and the aggregation of metallic nanoparticles are the common troubles. Here, the Au nanoparticles with uniform distribution on matrix have been achieved by dealloying method. Two kinds of Au/TiO_2 nanocomposites were prepared by calcination and hydrothermal synthesis of the dealloying induced Au/H-titanate precursor. The Au/TiO_2 nanocomposites present a mesoporous structure with large specific surface area. By comparison, the Au/TiO_2 nanocomposites obtained by calcination exhibit greatly enhanced photocatalytic activity for the degradation of methyl orange under irradiation of visible light. The homodisperse Au nanoparticles, large specific surface area and the well interaction between Au and TiO_2 are favorable for the enhanced visible light photocatalytic activity of Au/TiO_2 nanocomposites fabricated by calcination.

Introduction

Photocatalysis using sunlight has been attracting tremendous attention to solve energy and environmental crises.[1, 2] It is well known that visible light energy is far more abundant than ultraviolet light energy in the solar spectrum. Hence, tremendous efforts have been made to increase the visible-light response of wide-bandgap semiconductor nanostructures. TiO_2 as one of the most promising photocatalysts has been widely used in energy and environmental fields.[3] However, the lack of absorbance for visible light is a fatal drawback which greatly limits its application.[4] The localized surface plasmon resonance (LSPR) technology can tune the light response of TiO_2 from ultraviolet to visible light. In fact, the plasmonic metal/semiconductor hybrid nanostructures have recently attracted much attention because of their intriguing optical properties and enormous versatile technological applications.[5] When a noble metallic nanoparticle is excited by the certain wavelength of light, a strong oscillation of hot electrons happens on the noble metal surface. Generally speaking, Au, Ag, Pt and Pd nanostructures are good materials for LSPR in visible regions.[6] Au/TiO_2 composites (plasmonic Au nanoparticles modified TiO_2) have been used for degrading organic pollutants,[7] CO oxidation[8] and water splitting[9] under visible light.

Au/TO_2 composites can be prepared through the deposition or growth of metal nanostructures on pre-grown semiconductor nanostructures or by use of pre-grown metal nanostructures as seeds.[5] It is complex to fabricate the pre-grown metals or semiconductors through multiple steps with precisely controlled growth conditions.

The wet chemical methods,[10-13] such as hydrothermal, solvothermal, mixing noble metal colloidal solution with semiconductor dispersion, are the general and conventional methods for the incorporation of noble metal nanoparticles onto semiconductor. However, the aggregation of metal nanoparticles is the common suffered problem apart from the harsh reaction conditions using these methods, which leads to a significant decrease in the surface area available for the photocatalysis. How to simplify the preparation process with uniform distribution of noble metal nanoparticles is desired for manufacturing plasmonic metal/semiconductor photocatalysts.

According to some researches, [14, 15] a high surface area is also important to enhance the photocatalytic activity by increasing the number density of redox reaction sites on the surface. The O[16] and Ti[17] vacancies as the typical surface active sites are able to provide electrons and holes to react to oxygen and water molecules. These defects depend on the oxygen activity in the ambient atmosphere during annealing. There is no doubt that more defects will exist in the TiO_2 with a large specific surface area through calcination. The mesoporous anatase TiO_2 has been prepared by combining dealloying with calcination or hydrothermal synthesis, exhibiting well photocatalytic activities.[18] Dealloying (selective corrosion) is normally utilized to fabricate nanoporous metals/alloys/nanocomposites with high surface area.[19-21]

Here we developed a novel process for inducing Au nanoparticles in the mesoporous TiO_2 photocatalysts (Au/TiO_2 nanocomposites) with greatly enhanced photocatalytic activity through the combination of chemical dealloying with

calcination. In comparison, the hydrothermal treatment of the dealloying induced Au/H-titanate precursor was also adopted to fabricate the Au/TiO_2 nanocomposites with different microstructures and photocatalytic activity. The photocatalytic activities of the Au/TiO_2 nanocomposites were evaluated by degradation of methyl orange (MO) under visible light. Moreover, the related mechanisms have also been discussed with respect to the formation and photocatalysis of the Au/TiO_2 nanocomposites.

Experimental section

Preparation of the Au/TiO_2 nanocomposites

The alloying ingots with compositions of $Al_{97.1}Ti_{2.9}$ and $Al_{97.2}Ti_{2.77}Au_{0.03}$ were prepared by melting pure Al, Ti and Au metals (purity > 99.9 wt%) in a high-frequency induction furnace. The alloy ribbons were obtained using a single roller melt spinning instrument. The Au/Na-titanate (Na-titanate) was prepared by dealloying the $Al_{97.2}Ti_{2.77}Au_{0.03}$ ($Al_{97.1}Ti_{2.9}$) ribbons in a 4 mol/L NaOH aqueous solution under free corrosion conditions. Then the Au/H-titanate (H-titanate) was obtained after immersing Au/Na-titanate (Na-titanate) in a 0.1 mol/L HCl aqueous solution at room temperature for 2 h. By calcination of the H-titanate or Au/H-titanate at 400 ^oC for 2 h, the TiO_2-C or Au/TiO_2-C was successfully fabricated. The TiO_2-H or Au/TiO_2-H was prepared by a hydrothermal method. The hydrothermal procedure was described as follows. The H-titanate or Au/H-titanate was dispersed in the mixture of water and alcohol with equal volumes and stirred vigorously for 30 min using ultrasonic instrument. After adding 2 mL of dimethylamine into the mixture, the

stirring treatment was continued for another 30 min. Then the resulting mixture was sealed in a Teflon-lined stainless steel autoclave with a capacity of 50 mL and maintained at 160 ^{o}C for 12 h. Finally, the precipitates (Au/TiO_2-H or TiO_2-H) were washed by deionized water for several times.

Characterization

All products were characterized by X-ray diffraction (XRD, D8-advance, BRUKER), field emission scanning electron microscopy (FESEM, QUANTA FEG 250, FEI), transmission electron microscopy (TEM, JEM-2100, JEOL) with high-resolution transmission electron microscopy (HRTEM). The UV-vis diffuse reflectance spectra (DRS, UV-690, MAPADA) were recorded in a wavelength range of 250–800 nm to study the optical performance of the samples. Nitrogen adsorption-desorption isotherms were measured at -196 ^{o}C with a V-Sorb 2800P (GAPP, China) surface area and porosity analyzer. Brunauer-Emmett-Teller (BET) method was used to calculate the specific surface area. The pore size distribution was measured from the desorption branch of isotherm using the corrected form of Kelvin equation by the Barrett-Joyner-Halenda (BJH) method. Raman spectroscopy was performed with a LabRAM HR Evolution Raman system (HORIBA Scientific, λ = 633 nm). The X-ray photoelectron spectroscopy (XPS) was carried out with an ESCALAB 250 spectrometer and a monochromatic Al Kα X-ray source (150 W). All reported binding energy values were calibrated to the C 1s peak at 284.8 eV.

Photocatalytic experiment

The photocatalytic activities of the samples were evaluated by degradation of MO

aqueous solution at room temperature under visible light irradiation, because MO, as a typical chemically stable containing-nitrogen dye pollutant, is always regarded as the target degradation in photocatalysis field.[22] A 300 W xenon lamp with 420 nm cut-filter was used as the visible light source. The photocatalytic experiments under visible light irradiation were carried out by adding 10 mg photocatalysts (P25, TiO_2-C, TiO_2-H, Au/TiO_2-C or Au/TiO_2-H) into 25 mL MO solution (10 mg/L). The suspension was stirred in the dark for 20 min to obtain the saturated adsorption of MO before visible light illumination. At varied irradiation time intervals, the concentration of the MO solution was measured by monitoring the absorbance at 464 nm (the maximum absorbance wavelength of MO) using a UV-vis spectrophotometer (UV-3200pc, MAPADA). The catalytic activities were evaluated by the ratio of the concentration of MO after irradiation for different time (C) divided by the initial concentration (C_0) (i.e., C/C_0).

Results and discussion

Fig.1 presents the XRD patterns of the Au/Na-titanate, Au/H-titanate, and Au/TiO_2 samples. The peaks at 38.2°, 44.3°, 64.5° and 77.7° can be assigned to the face centered cubic (fcc) Au phase (marked by the diamond symbols on the XRD patterns). Obviously, the diffraction peaks of fcc Au are detected in each of the XRD patterns or in various stages of the material synthesis. The curves (a and b) are the typical XRD patterns of Au/Na-titanate and Au/H-titanate, respectively. Although the shapes of these two patterns are very similar, the different diffraction peak positions

and intensities (marked by arrows) of titanate change markedly before and after HCl treatment. The fluctuations of titanate diffraction peaks are due to the replacement of Na^+ in Na-titanate by H^+.[23, 24] Besides, the diffraction intensity of fcc Au increases in the XRD pattern of Au/H-titanate, suggesting that the grain size of metallic Au has changed during the acid treatment. The curves (c and d) are the XRD patterns of different Au/TiO_2 nanocomposites by calcination and hydrothermal treatment of Au/H-titanate samples. The anatase TiO_2 and fcc Au are detected in the two samples, illustrating the transformation from the H-titanate to TiO_2 during the calcination and hydrothermal processes.

Fig. 2 shows the FESEM images of the samples obtained at different stages. The Au/Na-titanate obtained by dealloying the Al-Ti-Au alloy ribbons presents typical 3D network structure (Fig. 2(a)). As shown in Fig. 2(b), the 3D network structure is still observed in Au/H-titanate, and the Au nanoparticles loading on the 3D network matrix can be distinguished. These results prove the rearrangement of Au atoms during HCl treatment, which is a common phenomenon in dealloying.[25] The grain size of fcc Au becomes larger after rearrangement, which has been displayed in the XRD result (Fig. 1(b)). Fig. 2(c) shows the morphology of the Au/TiO_2-C which was obtained by calcination of Au/H-titanate. The anatase TiO_2 matrix presents the similar 3D network structure to the H-titanate, and the Au nanoparticles distribute in the anatase TiO_2 matrix. Of interest, the size of the ligaments (network skeletons) becomes smaller than that of the Au/titanate, which is caused by the volumetric shrinkage induced by dehydration. In contrast, the Au/TiO_2-H prepared by hydrothermal treatment of

Au/H-titanate presents the spindle-like anatase TiO_2 matrix with Au nanoparticles on the surface (Fig. 2(d)). Obviously, the 3D network structure was destroyed during the hydrothermal treatment. The pure TiO_2 also presents the similar morphologies to these TiO_2 matrices of Au/TiO_2 composites (Fig. S1).

The TEM images (Fig. 3(a) and Fig. S2) of Au/TiO_2-C show that the Au nanoparticles with the size of 5~30 nm are uniformly embedded in the 3D network TiO_2 matrix without aggregations. The embedded Au nanoparticles in the anatase matrix indicate that the 3D network structure can effectively prevent the Au nanoparticles from aggregating at high temperature. The close investigation of the Au nanoparticles in Au/TiO_2-C is observed by HRTEM (Fig. 3(b)). The lattice spacings of 0.235 and 0.350 nm correspond to (111) plane of fcc Au and (101) plane of the anatase TiO_2, respectively. And the lattice fringes of major Au nanoparticles (Fig. 3(c and d)) are difficult to be observed as clear as Fig. 3(b). The Au nanoparticles are wrapped by the anatase TiO_2 matrix as shown in Fig. 3(a) and Fig. S2, causing the Au nanoparticles to be covered by the TiO_2 matrix. Fig. 3(d) shows a small amount of lattice fringes of an Au nanoparticle, proving the bridging effect of TiO_2 matrix with Au nanoparticles.

In contrast, the Au/TiO_2-H presents the different morphology (Fig. 4(a)). The aggregated Au nanoparticles (marked by dashed circles in Fig. 4(a) mix with the diamond-like and spindle-like anatase TiO_2 matrix. As shown in Fig. 4(a) and Fig. S3, the regular shaped anatase TiO_2 exists alone, not with the Au nanoparticles. The HRTEM images (Fig. 4(b)) show the regular shaped anatase TiO_2 with the lattice

spacing of 0.350 nm corresponding to (101) plane. The anatase TiO_2 matrix is formed by dissolution/recrystallization in hydrothermal process.[26, 27] As a result, Au nanoparticles fall off from the H-titante matrix. The deciduous Au nanoparticles are more inclined to get together under gravity during the hydrothermal process. The size of the Au nanoparticles in Au/TiO_2-H is similar to that in Au/TiO_2-C (Fig. 4(c and d)), indicating that the Au nanoparticles do not become larger during calcination.

Fig. 5 depicts the N_2 adsorption-desorption isotherms and the related pore size distribution curves, showing the BET specific surface area and porous characteristics of the Au/TiO_2 nanocomposites. The N_2 adsorption-desorption curves of these two Au/TiO_2 nanocomposites exhibit the type IV isotherm with a H3-type hysteresis loop, illustrating the mesoporous characteristic which is in accordance with the FESEM and TEM results. However, the formation mechanisms of mesoporous structure are different from each other for these two samples. The Au/TiO_2-C preserves the dealloying-driven 3D network structure with a large BET specific surface area (as high as 118 m^2/g) during the calcination. As for the Au/TiO_2-H, the mesoporous structure is formed due to the accumulation of anatase TiO_2 nanoparticles. The dissolution/recrystallization process destroys the 3D network structure resulting in decreasing the BET surface area to 81 m^2/g. The BJH pore-size distribution curve (insert of Fig. 5(a)) indicates that the Au/TiO_2-C possesses a narrow pore-size distribution with two kinds of pore diameters of 2 ~ 3 and 3 ~ 20 nm. In comparison, a broad pore distribution (2 ~ 100 nm) is observed in the Au/TiO_2-H samples (insert of Fig. 5(b)). The smaller specific surface area and the broader distribution of pore

diameters in Au/TiO_2-H are due to the destruction of 3D network structure.

Fig. 6(a) shows the DRS of the Au/TiO_2 nanocomposites. The resultant Au/TiO_2 nanocomposites display different color (inserts of Fig. 6(a)), indicating Au modified TiO_2 can absorb visible light. The DRS curves of the Au/TiO_2 nanocomposites exhibit strong LSPR absorption peaks at about 550 nm. The LSPR absorption peak of the Au/TiO_2-C is centered at 554 nm, ~4 nm longer than the peak of the Au/TiO_2-H. Almost the same wavelength of LSPR absorption indicates the same size of Au nanoparticles in these two samples.[28] The plots of $(F(R)E)^{1/2}$ versus the energy of absorbed light are converted from the UV-vis DRS according to the Kubelka–Munk function (Fig. 6(b)).[29] The bandgap energies of the Au/TiO_2 nanocomposites estimated from the intercept of the tangent to the plot are around 2.97 eV, which are lower than 3.16 eV of P25. It is obvious that the narrower energy gap of Au/TiO_2 is beneficial to absorb the photons with lower energy. Besides, the pure TiO_2 samples obtained by our methods also exhibit the absorption for visible light (Fig. S4).

Fig. 7 shows the Raman spectra of commercial TiO_2 (P25) and Au/TiO_2 nanocomposites. The observed characteristic E_g, B_{1g} and A_{1g} Raman peaks confirm the anatase structure in Au/TiO_2 and P25. Of importance, the characteristic E_g peak shifts to a higher wavenumber after Au modifying the anatase TiO_2 (insert of Fig. 7), demonstrating the increased crystalline defects within the anatase TiO_2.[30] These crystalline defects, formed at the contact region of Au and TiO_2, influence the vibrational frequency of the anatase TiO_2 and act as traps to capture photoelectrons.

Photocatalytic activities of the photocatalysts (P25, pure TiO_2 and Au/TiO_2) were

further investigated by decomposition of MO aqueous solution under visible light irradiation. According to the experimental results (Fig. S5), the optimum dosage of photocatalysts was determined to be 10 mg. Fig. 8(a) shows the degradation efficiencies (C/C_0) of different catalysts (Au/TiO_2-C, Au/TiO_2-H and P25) as a function of irradiation time. The remarkable visible light-promoted activity is obtained only for the Au/TiO_2-C sample. After irradiation of 90 min under visible light, MO solution is almost completely degraded by the Au/TiO_2-C nanocomposites. But similar to P25 (commercial TiO_2 catalyst), the Au/TiO_2-H presents the poor photocatalytic activity. So the Au nanoparticles are not the depending factor in enhanced photocatalytic activity. This can also be proved by the comparison of photocatalytic efficiencies between TiO_2-H and Au/TiO_2-H (Figs. S6 and S7). The crucial factors should be the close contact (such as Schottky contact) between Au and TiO_2.[31] As shown in Fig. 8(b), the intensity of the MO absorbance decreases with increasing the treatment time and no additional peaks appear, indicating that the MO molecules can be adsorbed and degraded by the Au/TiO_2-C. And the UV-Vis absorption spectrum of MO solution is slightly red-shifted after treatment in dark due to the acid condition. The UV-vis absorption spectra of MO solution using other photocatalysts are shown in Fig. S6. Clearly, the different TiO_2 catalysts (TiO_2-H and TiO_2-C) present the similar photocatalytic activity under visible light, which agrees with the DRS results (Fig. S4).

Fig. 9 depicts the high resolution XPS spectra of the Au/TiO_2-C. The Ti, O, Au and Cl elements are detected on the XPS survey of Au/TiO_2-C as shown in Fig. S8.

According to the results, the Ti 2p spectrum is dominated by species in the Ti^{4+} oxidation state (Fig. 9(a)). The XPS peaks separation of 5.7 eV between two Ti 2p states is also the characteristic of Ti^{4+} oxidation state. As reported in the case of oxides, the binding energies of the lattice oxygen (O^{2-}, 529.9 eV) and the surface OH species (531.6 eV) are shown in Fig. 9(b).[32, 33] The co-existence of Ti^{4+} and O^{2-} further confirms the formation of TiO_2 in the Au/TiO_2-C. As shown in Fig. 9(c), the Au 4f spectrum is composed of two peaks at binding energies of 82.98 and 86.68 eV and the separation between two peaks is 3.7 eV, suggesting that the Au species in the samples is metallic state.[34] Compared to Au^0 $4f_{7/2}$ (84.0 eV),[35] the negative shift of Au peak is attributed to the intimate contact between Au and the defect site on the TiO_2 surface.[36] The Ti/Au atomic ratio is about 100/1 according to the XPS results which approximately equals to the ratio of 92/1 in original Al-Ti-Au ribbons. In addition, the weak signal of Cl^- ions exhibits two peaks at 199.9 and 201.3 eV for Cl $2p_{3/2}$ and Cl $2p_{1/2}$, respectively.[37, 38] Cl^- ions may be adsorbed on the Au/H-titanate samples after acid treatment in the HCl solution.[39, 40] The absorbed Cl^- ions cause the slight red-shift of the MO absorption spectrum in Fig. 8(a) due to the acid environment.

The Au/TiO_2-C exhibits the greatly enhanced photocatalytic activity by comparing with P25. However, the Au/TiO_2-H presents poor activity, which is closely related to the fabrication process. Fig. 10 illustrates the formation and the photocatalytic mechanism of the Au/TiO_2 nanocomposites. The Au/H-titanate with 3D network structure is fabricated by dealloying and acid treatment. The Au nanoparticles are evenly dispersed in the titanate matrix at the dealloying stage. The dehydration

causes the formation of 3D network anatase TiO_2 during the calcination of Au/H-titanate at 400 ^oC. In addition, the 3D network structure prevents the Au nanoparticles from aggregating and anchors them in their original positions. Of importance, the calcination process promotes the close contact between Au nanoparticles and the anatase TiO_2 matrix, which is propitious to the Schottky contact.[41] However, the H-titanate dissolves during the hydrothermal process, which causes the Au nanoparticles falling off from the matrix. In addition, the white (anatase TiO_2) and atropurpureus (Au nanoparticles) products were found together in the Au/TiO_2-H after hydrothermal treatment, which proved the falling off Au nanoparticles from the matrix. The deciduous Au nanoparticles are easy to get together. At the recrystallization stage, the spindle-like and diamond-like anatase TiO_2 particles are very difficult to combine with the Au nanoparticles. Therefore, the Au/TiO_2-H is similar to the photocatalysts obtained by simply mixing the Au nanoparticles with TiO_2 matrix. Hence, hydrothermal treatment is difficult to form a solid interface between Au and TiO_2.

It is clear that the Au/TiO_2-H and Au/TiO_2-C samples exhibit the absorption for visible light, but the photodegradation abilities are different. When Au/TiO_2-C is exposed to visible light, the electrons below the Fermi level (E_f) of the Au nanoparticles are excited to the surface plasma, leaving positive charges (h^+) below the E_f. Then the excited electrons transfer to the TiO_2 matrix due to its strong electron oscillating collectively on the LSPR excitation. The electrons are trapped by O_2 to form superoxide radical ion ($\cdot O_2^-$) and holes react with adsorbed H_2O to form the ·OH.

These radicals ($\cdot O_2^-$ and $\cdot OH$) are very powerful for the degradation of MO molecules.[42] Although Au nanoparticles can be excited to the LSPR in Au/TiO_2-H, the excited charges cannot be separated due to the poor contact between Au and TiO_2. Therefore, the absorbed light may transform to the other energy by Au/TiO_2-H. The extremely uneven distribution of Au nanoparticles in Au/TiO_2-H sample decreases the surface area available for the photocatalytic reaction. The extremely uneven distribution of Au nanoparticles and poor contact between Au and TiO_2 bring about the relatively poor photocatalytic activity of Au/TiO_2-H.

Conclusions

In summary, the Au/TiO_2 nanocomposites with high surface area can be fabricated by combining the chemical dealloying/HCl treatment with calcination or hydrothermal synthesis. The Au nanoparticles uniformly distributed in the H-titanate matrix with 3D network structure have been achieved by dealloying and subsequent HCl treatment at room temperature. The Au/TiO_2 nanocomposites with monodisperse Au nanoparticles embedded in the 3D mesoporous network can be prepared by the calcination of Au/H-titanate. In addition, the calcination process prevents the aggregation of Au nanoparticles and promotes the close contact between the Au nanoparticles and anatase TiO_2 matrix. The hydrothermal treatment of Au/H-titanate leads to the formation of the Au/TiO_2 nanocomposites with spindle-like and diamond-like TiO_2 matrix. However, the hydrothermal treatment destroys the 3D network structure and results in the poor contacts between aggregated Au

nanoparticles and TiO_2 matrix. Compared to the commercial P25, the Au/TiO_2 nanocomposites fabricated by calcination exhibit the greatly enhanced photocatalytic activity under visible light irradiation. The enhanced photocatalytic activity is attributed to the Au nanoparticles with uniform distribution, the 3D network structure with high surface area and the close contact between Au and TiO_2.

Acknowledgements

The authors acknowledge financial support from the National Natural Science Foundation of China (No. 51171072 and No. 51401085), and Key Research Development Program of Shandong Province of China (No. 2015GGx102016).

References

[1] P. Zhou, J. Yu and M. Jaroniec, *Adv. Mater.,* 2014, **26**, 4920-4935.

[2] L. Liu, S. Ouyang and J. Ye, *Angew. Chem. Int. Ed.,* 2013, **52**, 6689-6693.

[3] H. Tada, T. Kiyonaga and S. Naya, *Chem. Soc. Rev.,* 2009, **38**, 1849-1858.

[4] Z. Zhao, J. Tian, Y. Sang, A. Cabot and H. Liu, *Adv. Mater.,* 2015, **27**, 2557-2582.

[5] R. Jiang, B. Li, C. Fang and J. Wang, *Adv. Mater.,* 2014, **26**, 5274-5309.

[6] Y. Qu and X. Duan, *Chem. Soc. Rev.,* 2013, **42**, 2568-2580.

[7] X. Pan and Y. Xu, *J. Phys. Chem. C,* 2013, **117**, 17996-18005.

[8] Y. Maeda, Y. Iizuka and M. Kohyama, *J. Am. Chem. Soc.,* 2013, **135**, 906-909.

[9] Z. Zhan, J. An, H. Zhang, R. V. Hansen and L. Zheng, *ACS Appl. Mater. Interfaces,* 2014, **6**, 1139-1144.

[10] Q. Zhang, D. Lima, I. Lee, F. Zaera, M. Chi and Y. Yin, *Angew. Chem. Int. Ed.,* 2011, **50**, 7088-7092.

[11] J. Chen, J. Wu, P. Wu and D. P. Tsai, *J. Phys. Chem. C,* 2011, **115**, 210-216.

[12] Y. Lu, H. Yu, S. Chen, X. Quan and H. Zhao, *Environ. Sci. Technol.,* 2012, **46**, 1724-1730.

[13] Y. Tang, Z. Jiang, Q. Tay, J. Deng, Y. Lai, D. Gong, Z. Dong and Z. Chen, *RSC Adv.,* 2012, **2**, 9406-9414.

[14] K. Maeda and K. Domen, *J. Phys. Chem. C,* 2007, **111**, 7851-7861.

[15] J. Joo, Q. Zhang, I. Lee, M. Dahl, F. Zaera and Y. Yin, *Adv. Funct. Mater.,* 2012, **22**, 166-174.

[16] M. Setvín, U. Aschauer, P. Scheiber, Y. Li, W. Hou, M. Schmid, A. Selloni and U.

Diebold, *Science,* 2013, **341**, 988-991.

[17] J. Nowotny, T. Bak, M. K. Nowotny and L. R. Sheppard, *J. Phys. Chem. B,* 2006, **110**, 18492-18495.

[18] Z. Zhao, J. Xu, C. Shang, R. Ye and Y. Wang, *Corros. Sci.,* 2015, **98**, 651-660.

[19] J. Sun, J. Shi, J. Xu, X. Chen, Z. Zhang and Z. Peng, *J. Power Sources,* 2015, **279**, 334-344.

[20] Z. Zhang, C. Zhang, J. Sun, T. Kou, Q. Bai, Y. Wang and Y. Ding, *J. Mater. Chem. A***,** 2013, **1**, 3620-3628.

[21] Z. Zhang, C. Zhang, J. Sun, T. Kou and C. Zhao, *RSC Adv.*, 2012, **2**, 11820-11828.

[22] Y. Liao, H. Zhang, Z. Zhong, L. Jia, F. Bai, J. Li, P. Zhong, H. Chen and J. Zhang, *ACS Appl. Mater. Interfaces,* 2013, **5**, 11022-11028.

[23] J. Yang, Z. Jin, X. Wang, W. Li, J. Zhang, S. Zhang, X. Guo and Z. Zhang, *Dalton Trans.,* 2003, **20**, 3898-3901.

[24] R. Ma, T. Sasaki and Y. Bando, *Chem. Commun.,* 2005, 948-950.

[25] J. Erlebacher, M. J. Aziz, A. Karma, N. Dimitrov and K. Sieradzki, *Nature,* 2001, **410**, 450-453.

[26] H. K. Wang, W. Shao, F. Gu, L. Zhang, M. K. Lu and C. Z. Li, *Inorg. Chem.,* 2009, **48**, 9732-9736.

[27] Y. Qiu, K. Yan, S. Yang, L. Jin, H. Deng and W. Li, *ACS Nano,* 2010, **4**, 6515-6526.

[28] R. Zanella, S. Giorgio, C. Shin, C. R. Henry and C. Louis, *J. Cata.,* 2004, **222**,

357-367.

[29] H. Huang, D. Li, Q. Lin, Y. Shao, W. Chen, Y. Hu, Y. Chen and X.i Fu, *J. Phys. Chem. C,* 2009, **113**, 14264-14269.

[30] Y. Li, H. Wang, Q. Feng, G. Zhou and Z. Wang, *Energy Environ. Sci.,* 2013, **6**, 2156-2165.

[31] R. Long, K. Mao, M. Gong, S. Zhou, J. Hu, M. Zhi, Y. You, S. Bai, J. Jiang, Q. Zhang, X. Wu and Y. Xiong, *Angew. Chem. Int. Ed.,* 2014, **53**, 3205-3209.

[32] G. Cappelletti, S. Ardizzone, C. L. Bianchi, S. Gialanella, A. Naldoni, C. Pirola and V. Ragaini, *Nanoscale Res. Lett.,* 2009, **4**, 97-105.

[33] A. Naldoni, M. Allieta, S. Santangelo, M. Marelli, F. Fabbri, S. Cappelli, C. L. Bianchi, R. Psaro and V. D. Santo, *J. Am. Chem. Soc.,* 2012, **134**, 7600-7603.

[34] K. Cheng, W. Sun, H. Jiang, J. Liu and J. Lin, *J. Phys. Chem. C,* 2013, **117**, 14600-14607.

[35] Z. Zheng, B. Huang, X. Qin, X. Zhang, Y. Dai and M. Whangbo, *J. Mater. Chem.,* 2011, **21**, 9079-9087.

[36] Z. Pei, L. Ding, W. Feng, S. Weng and P. Liu, *Phys. Chem. Chem. Phys.,* 2014, **16**, 21876-21881.

[37] A. Abidli, S. Hamoudi and K. Belkacemi, *Dalton Trans.,* 2015, **44**, 9823-9838.

[38] M. Dulski, K. Bilewska, M. Wojtyniak, J. Szade, J. Kusz, A. Nowak, R. Wrzalik, J. Kubacki and E.V. Galuskin, *Mate. Res. Bull.,* 2015, **70**, 920-927.

[39] C. Y. Teh, T. Wu and J. Ching, *Catal. Today,* 2015, **256**, 365-374.

[40] M. Hakamada and M. Mabuchi, *Nano Lett.,* 2006, **6**, 882-885.

[41] D. Ding, K. Liu, S. He, C. Gao and Y. Yin, *Nano Lett.,* 2014, **14**, 6731-6736.

[42] Y. Wen, H. Ding and Y. Shan, *Nanoscale,* 2011, **3**, 4411-4417.

Figures

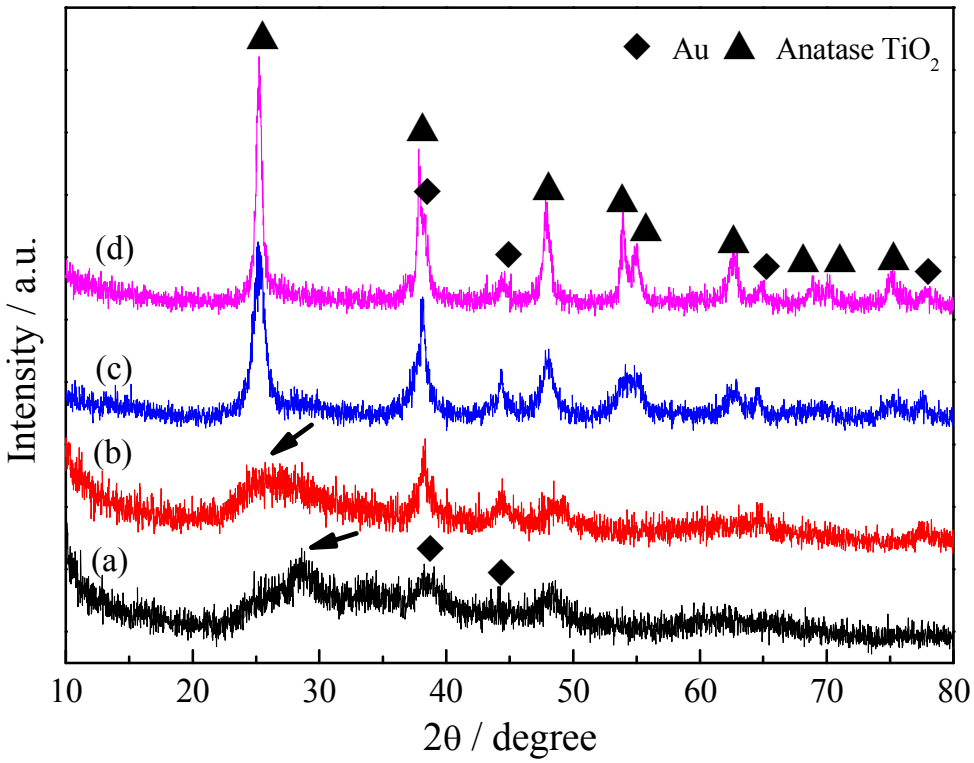

Fig. 1 XRD patterns of the samples. (a) Au/Na-titanate, (b) Au/H-titanate, (c) Au/TiO_2-C, (d) Au/TiO_2-H.

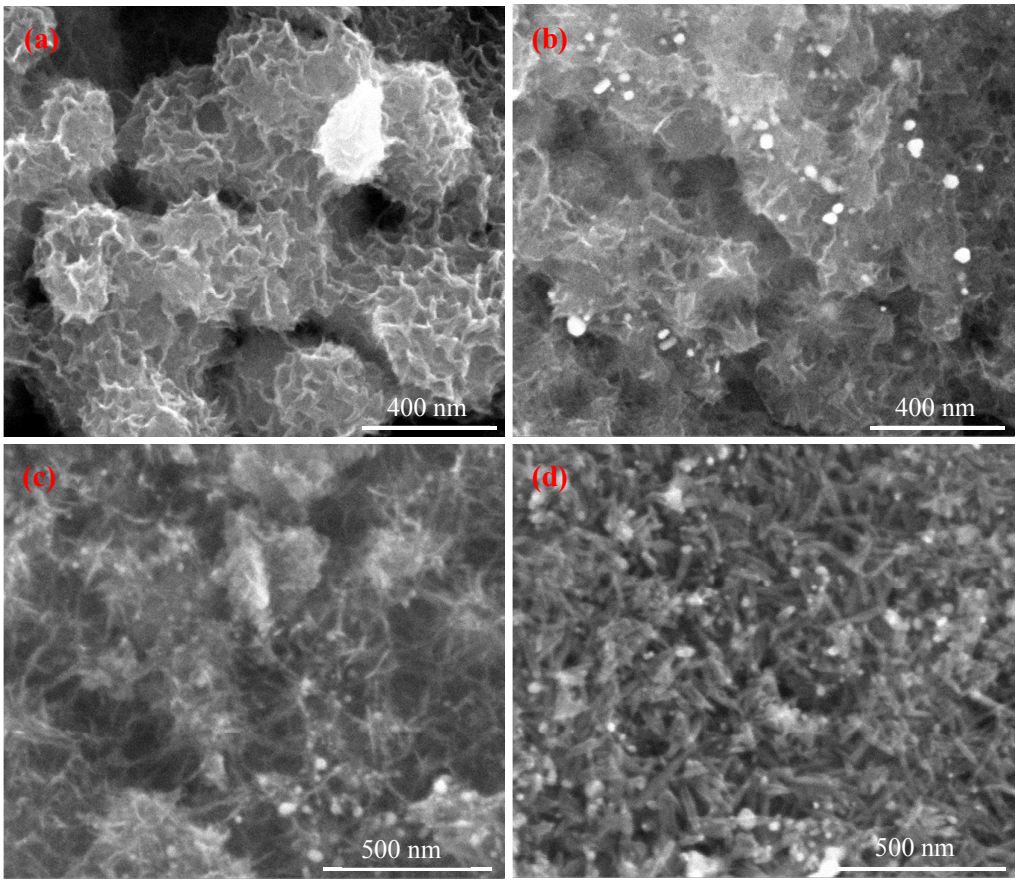

Fig. 2 FESEM images of the samples. (a) Au/Na-titanate, (b) Au/H-titanate, (c) Au/TiO_2-C, (d) Au/TiO_2-H.

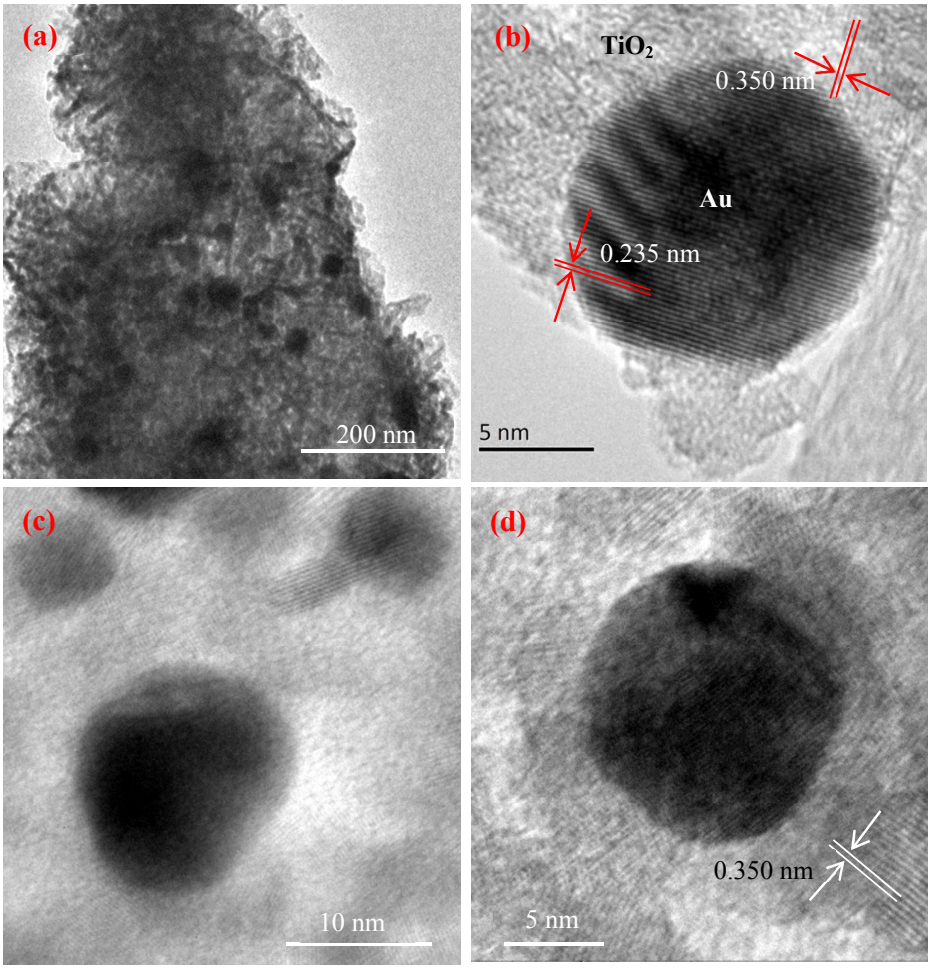

Fig. 3 (a) TEM image of the Au/TiO_2-C sample, and (b, c and d) the HRTEM images of the Au nanoparticles and the anatase TiO_2 matrix.

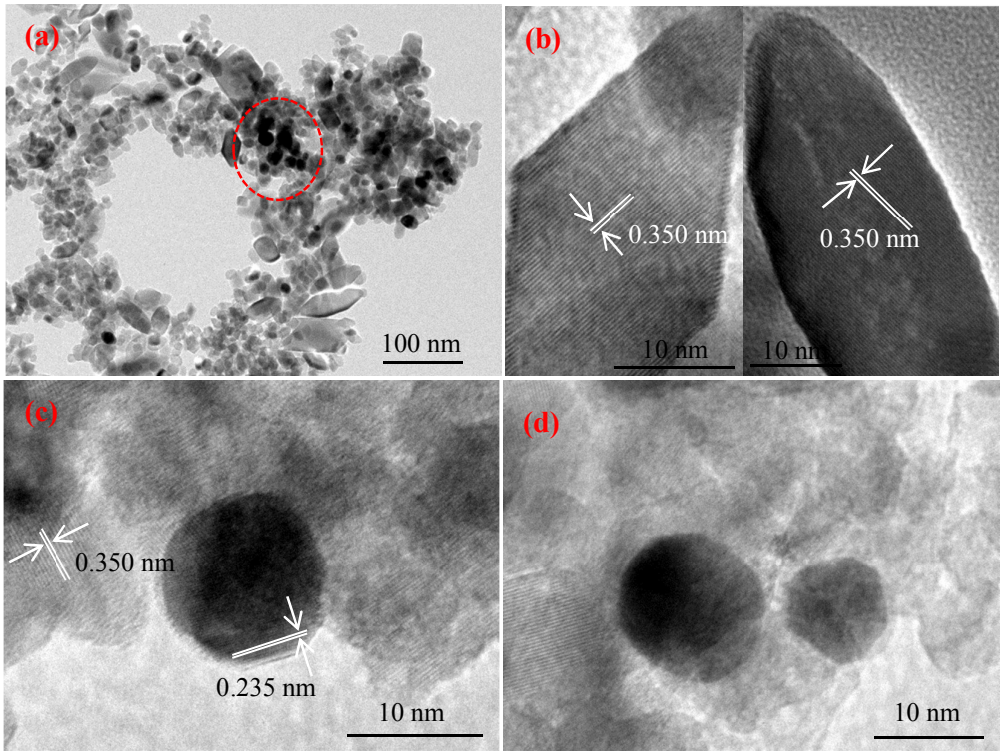

Fig. 4 (a) TEM image of the Au/TiO_2-H sample, (b) HRTEM images of the anatase TiO_2 matrix, and (c and d) HRTEM images of the Au nanoparticles in the TiO_2 matrix.

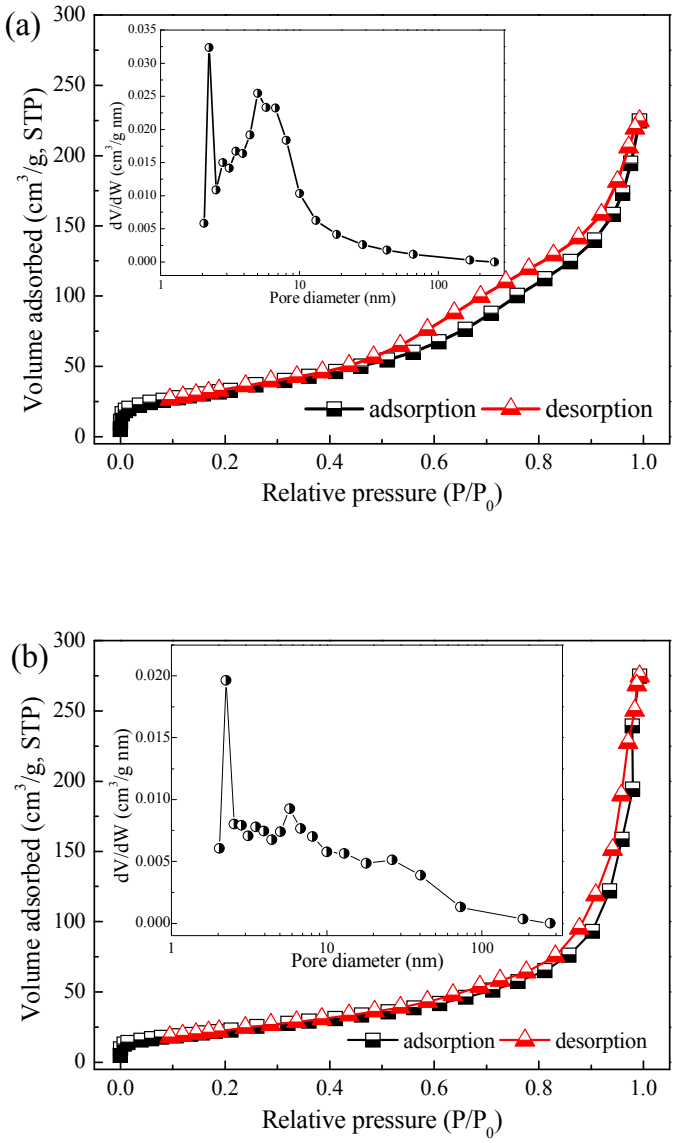

Fig. 5 N_2 adsorption-desorption isotherms and pore size distributions (inserts) of (a) Au/TiO_2-C and (b) Au/TiO_2-H.

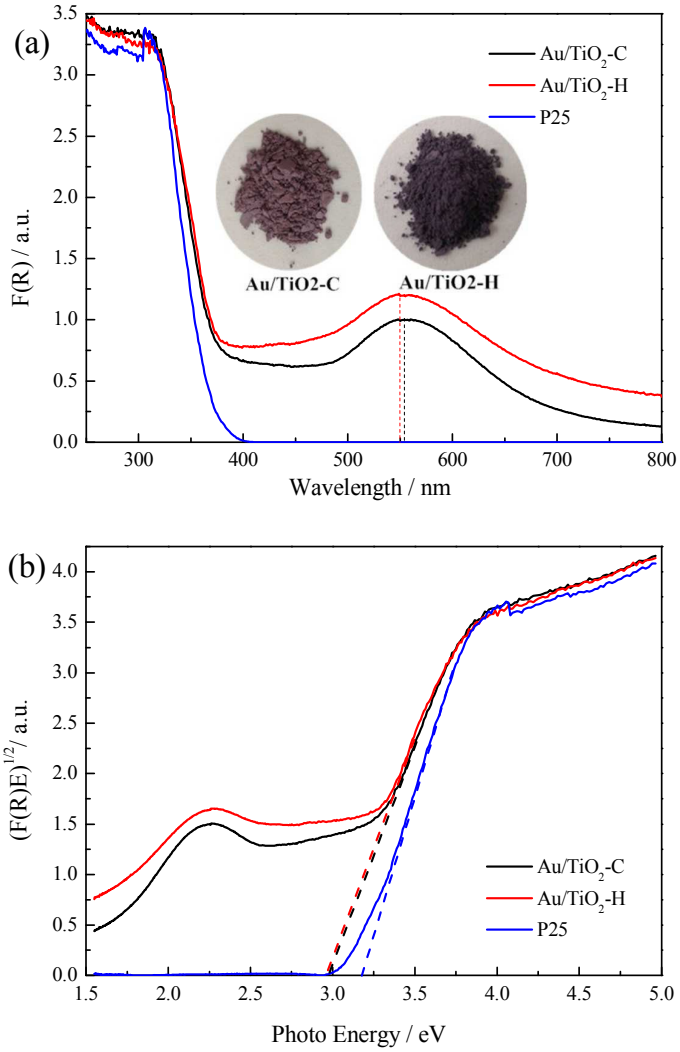

Fig. 6 UV-Vis diffuse reflectance spectra (DRS) of different photocatalysts and (b) plots transformed according to the Kubelka-Munk function versus energy of light for the photocatalysts. (insert in (a)) Photographs of the Au/TiO_2-C and Au/TiO_2-H powders.

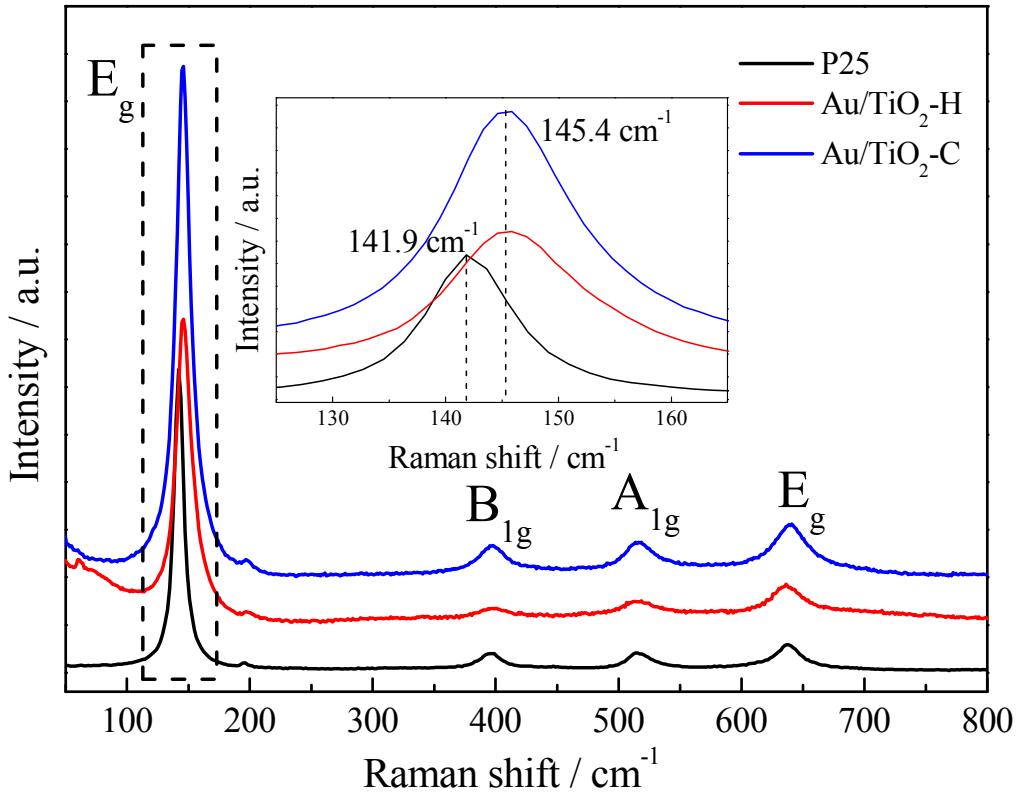

Fig. 7 Raman spectra of pure TiO_2 (P25) and Au/TiO_2 nanocomposites fabricated by different synthetic methods. (Insert) Enlarged plot of the E_g peaks of different photocatalysts.

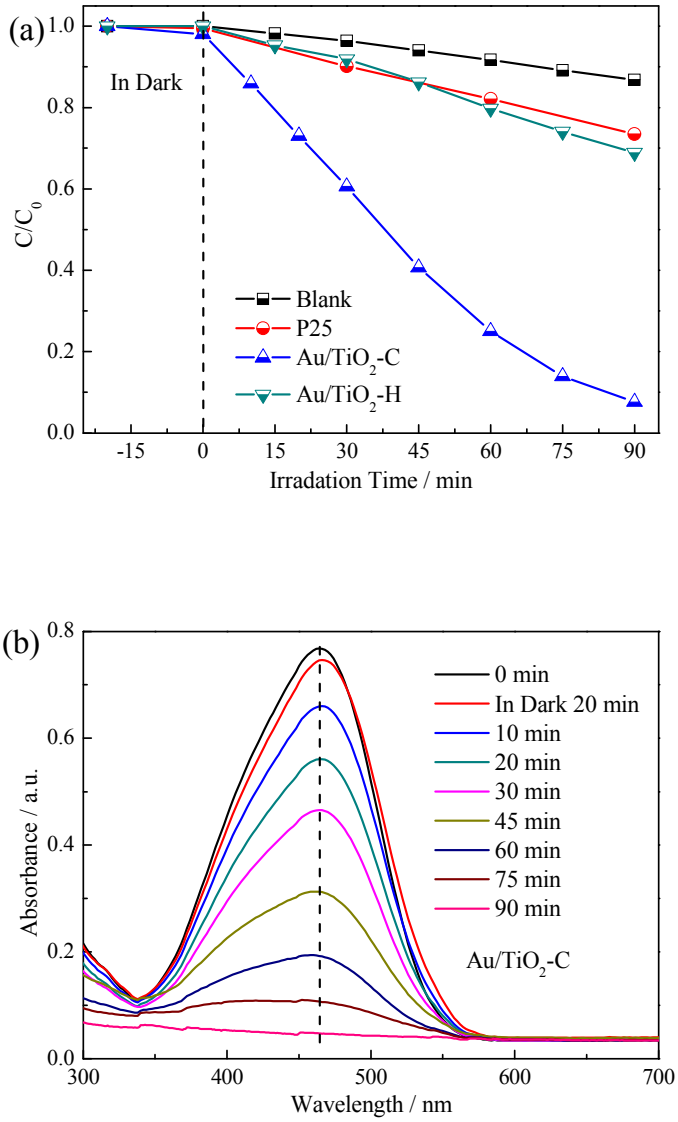

Fig. 8 (a) Comparison of photocatalytic activities of different photocatalysts. (b) UV-vis absorption spectra of MO solution under different visible light irradiation time in the presence of Au/TiO_2-C.

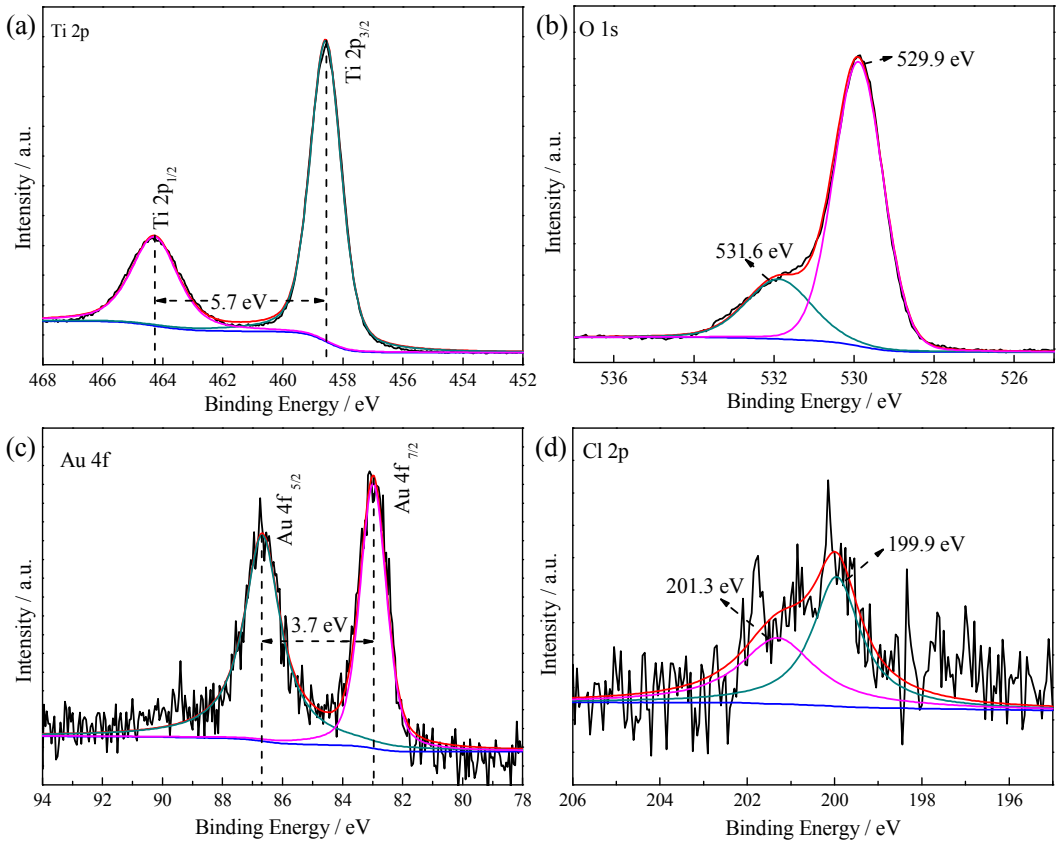

Fig. 9 XPS spectra of Au/TiO_2-C. (a) Ti 2p, (b) O 1s, (c) Au 4f and (d) Cl 2p.

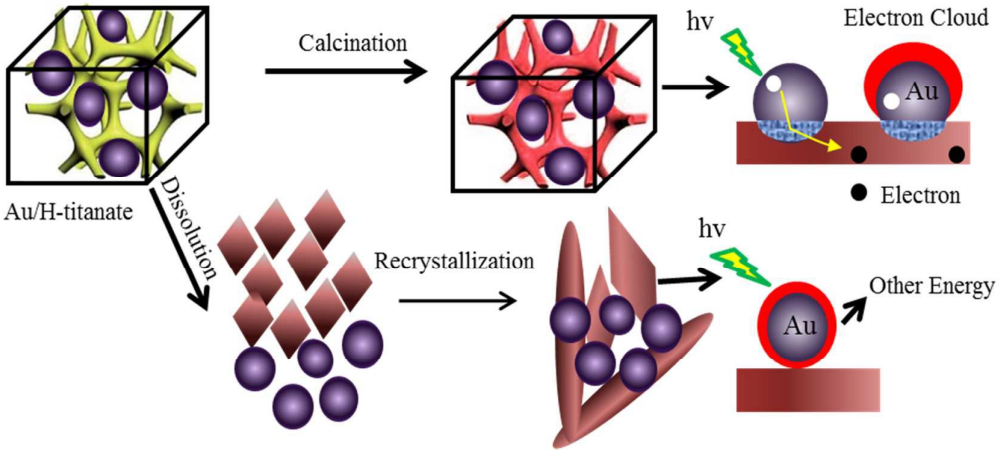

Fig. 10 Schematic illustration showing the formation mechanism and photocatalytic mechanism of the Au/TiO_2 nanocomposites.

Graphical abstract:

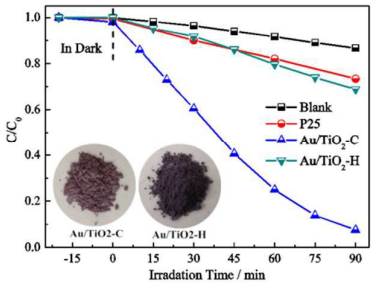

Au/TiO_2 nanocomposites with enhanced photocatalytic activity were fabricated by calcination or hydrothermal treatment of Au/H-titanate obtained through dealloying Al-Ti-Au alloy.